coatings MDPI

Thermal-Resistant Polyurethane/Nanoclay Powder Coatings: Degradation Kinetics Study

Maryam Jouyandeh [1] , Behzad Shirkavand Hadavand [2],*, Farimah Tikhani [3], Reza Khalili [4], Babak Bagheri [5] , Payam Zarrintaj [6] , Krzyszof Formela [7],* , Henri Vahabi [1] and Mohammad Reza Saeb [1]

1   Université de Lorraine, CentraleSupélec, LMOPS, F-57000 Metz, France;
    maryam.jouyande@gmail.com (M.J.); henri.vahabi@univ-lorraine.fr (H.V.); mrsaeb2008@gmail.com (M.R.S.)
2   Department of Resin and Additives, Institute for Color Science and Technology, Tehran 16765-654, Iran
3   School of Chemical Engineering, College of Engineering, University of Tehran, Tehran 11155-4563, Iran;
    farimah.tikhani@gmail.com
4   Polymer Engineering Department, Faculty of Engineering, Urmia University, Urmia 5756151818, Iran;
    khalili.polymer@gmail.com
5   Department of Chemical and Biomolecular Engineering, Korea Advanced Institute of Science and
    Technology (KAIST), Daejeon 34141, Korea; babakbagheri@kaist.ac.kr
6   School of Chemical Engineering, Oklahoma State University, 420 Engineering North, Stillwater, OK 74078,
    USA; payam.zarrintaj@okstate.edu
7   Department of Polymer Technology, Faculty of Chemistry, Gdańsk University of Technology,
    Gabriela Narutowicza 11/12, 80-233 Gdańsk, Poland
*   Correspondence: shirkavand@icrc.ac.ir (B.S.H.); krzysztof.formela@pg.edu.pl (K.F.);
    Tel.: +98-21-2295-6209 (B.S.H.); Fax: +98-21-2294-7537 (B.S.H.)

check for updates

Abstract: In the present study, thermal degradation kinetics of polyurethane (PU) powder coatings reinforced with organo-modified montmorillonite (OMMT) was investigated. PU nanocomposites were prepared in different concentrations of 1, 3, and 5 wt.% of OMMT via the extrusion method. The microstructure of the nanocomposites was observed by scanning electron microscope (SEM) illustrating uniform dispersion of OMMT nano-clay platelets in the PU matrix except for the sample containing 5 wt.% nano-palates. Thermal degradation kinetics of the PU nanocomposite was investigated using thermogravimetric analysis (TGA) at different heating rates of 5, 10, and 20 °C/min. The results showed that the initial decomposition temperatures were shifted toward higher values (more than 40 °C for $T_{5\%}$ and up to 20 °C for $T_{10\%}$) by introducing the nano-clay to the PU matrix. *Friedman*, *Kissinger–Akahira–Sunose* (*KAS*), *Flynn–Wall–Ozawa* (*FWO*), and modified *Coats-Redfern* iso-conversional methods were applied to model the decomposition reaction and the activation energy of the nanocomposite powder coatings. Overall, the presence of nano-clay increased the activation energy of the PU degradation up to 45 kJ/mol, when compared to the blank PU, which suggests very high thermal stability of nanocomposites. The *Sestak-Berggren* approach proposed a good approximation for the reaction model, especially at low temperatures. Thus, PU decomposition was detected as an autocatalytic reaction, which was suppressed by the barrier effect of OMMT nano-palates intercalated with polymer chains.

Keywords: polyurethane powder coating; nano-clay; thermogravimetric analysis; iso-conversional methods; degradation kinetics

1. Introduction

All the polymers exposed to the environmental conditions are highly susceptible to undergo degradation over the long-term. Consequently, their protection has drawn a great interest in order to prolong their lifetime, particularly for insulation and outdoor applications [1,2]. Developing proper methods of protection is pertinent to the comprehensive understanding of reactions taking place when the polymer is subject to destructive conditions. In the case of thermoset polymers under well-defined conditions, there is a direct relationship between the cross-linking density and network degradation. Normally, the thermal stability of polymer increases with densification of the thermoset network. In other terms, the denser the polymeric network, the lower the chain segment mobility, which hinders the diffusion of small molecules into the cross-linked system, according to Eyring theory [3]. Therefore, every factor that affects the cross-linking density of the polymer should be taken into account when it comes to studying the degradation kinetics in order to evaluate the underlying reaction mechanisms.

Some polymers like polyurethane (PU) inherently show a good resistance against oxygen, ozone, sunlight, oil, solvent, and fat, while their lack of thermal stability confines their applicability and induces fire risks [4,5]. Addition of nanoparticles to the polymers, even in a small amount, can markedly affect the cross-linking density of the final polymeric network, Consequently, this is their final performance [6]. Thus, different types of nanoparticles have been introduced to PU with the aim of preventing thermally-driven degradation of polymers by manipulating their microstructure, among which mineral nanoplatelets are widely common [7–9]. There are several reports indicating the role of nano-clay in improving the thermal properties of the PU. For example, a series of PU/organo-modified montmorillonite (OMMT) nanocomposites prepared by in-situ polymerization show enhanced decomposition temperature, according to the results presented by Rehab et al. [10]. In another study, Yang et al. [11] prepared PU nanocomposites of OMMT clay in different concentrations by a solution casting method. Thermal analysis revealed that the initial decomposition temperature of the nanocomposites has considerably increased (more than 25 °C), which has been ascribed to hydrogen bonding interaction between the OMMT and the polymer matrix. Moreover, Wang et al. [12] reported preparation of thermoplastic PU (TPU)/clay (Closite 30B) nanocomposite foams using the microcellular injection molding process. They found that the presence of clay nano-palates resulted in higher fire-retardancy and thermal stability with an 18-fold increase in char yield compared to the unfilled TPU sample due to the hindrance effect of OMMT on the diffusion and escape of gaseous products to the interior layers of the nanocomposite.

To be familiar with the thermal behavior of this coating material, a combination of experimental and computational investigations is a promising approach that makes it possible to correlate the polymer microstructure with its degradation kinetics. Thermogravimetric analysis (TGA) is a technique to directly track the relative changes in degradation kinetics of the polymer and monitor the integral alteration process of solid material to volatile compounds and residual char as degradation products [13,14]. Jomaa et al. [14] took advantage of this method to evaluate degradation kinetics of polyurethane pyrolysis and applied *Friedman* and *Kissinger* model-free methods to calculate the activation energy of the reaction. Both of the iso-conversional methods presented similar results with a slight difference attributed to the dissimilar mathematical treatments. Pashaei et al. [15] used the same method to investigate thermal degradation kinetics of PU/OMMT nanocomposites using three mathematical models of Horowitz-Metzger, Coats-Redfern, and Broido. They calculated the kinetic parameters and observed the increase of effective activation energy of their degradation reaction, which indicates the enhanced thermal stability. Likewise, Zhao et al. [16] applied Broido and Flynn-Wall-Ozawa (*FWO*) methods in order to deal with thermal oxidation kinetics of PU/OMMT nanocomposites, which resulted in improved thermal properties due to the good compatibility of interface between the nano-palates and matrix. Moreover, it was revealed that the presence of air induces complications to the oxidative degradation kinetics beside the complexity caused by barrier effect of OMMT, according to which the *FWO* model appeared to be more suitable for this purpose. Additional oxidative reactions are involved in the decomposition process of PU under air atmosphere, which can change the kinetic properties [17].

As a result, conducting thermal experiments under inert environment would moderately eliminate confusion and inaccuracy in studying the thermal decomposition kinetics of the polymer.

The goal of the present study is to investigate and develop thermal-resistant PU powder coatings reinforced with Cloisite 15A clay nanoplatelets as well as modeling thermal behavior and kinetics of degradation of powder coatings using non-isothermal TGA. To deepen the understanding of the degradation mechanism of PU/clay powder coatings, iso-conversional model-free methods were applied to the experimental data in order to calculate the kinetic parameters, such as the activation energy and frequency factor. The alteration of the activation energy of the pyrolysis reaction by partial mass loss was also captured by *Friedman*, *FWO*, Kissinger–Akahira–Sunose (*KAS*), and the modified Coats-Redfern (*m-CR*) methods.

2. Materials and Methods

In this research polyurethane powder coating (9016 WU18AX) manufacture of Peka Chimie Company (Tehran, Iran) with curing agent of Vestagon B 1530 from Evonik Resource Efficiency GmbH (Darmstadt, Germany) was used. Additionally, nanoclay Cloisite 15A purchased from US Research Nanomaterials Inc (Houston, TX, USA). Cloisite 15 is a bis (hydrogenated tallow alkyl) dimethyl salt with bentonite.

2.1. Preparation of Polyurethane Nanocomposite

PU-base powder coatings with 1, 3, and 5 wt.% of nano-clay were prepared in the twin screw extruder (Yantai Donghui Powder Processing Equipment Company, Yantai, China) under screw speed of 180 rpm and hopper temperature of 90 °C for preparing chips of nanocomposites. Then, chips were powdered and sieved to an average particle size of 55 μm. Prepared powder nanocomposites were coated on 10 × 15 cm metal plates by an electrostatic method and cured at 180 °C for 20 min.

2.2. Characterization

2.2.1. Scanning Electron Microscopy

The morphology and the dispersion state of clay nanoplates in the PU matrix was imaged by scanning electron microscopy (SEM). For this purpose, the cross section of the fractured surface of PU/clay nanocomposite powder coatings was analyzed by Hitachi S-4160 SEM (Tokyo, Japan).

2.2.2. Thermal Decomposition Characterization

Thermal behavior and kinetics of degradation of PU/clay nanocomposite powder coatings were investigated by using the Setaram Labsys Evo thermogravimetric analyzer (Setaram Labsys TM, Caluire, France). In order to remove moisture of the PU and PU/clay nanocomposites, all the samples were dried prior to TGA investigation at 60 °C for 12 h. Decomposition measurement was performed in the temperature range of 25–800 °C at heating rates of 5, 10, and 20 °C/min under nitrogen atmosphere with a flow rate of 100 cm^3/min.

2.3. Methods

The TGA data were analyzed as the percentage of weight loss expressed as a function of temperature. In order to study the thermal degradation behavior, the degree of thermal degradation (α) was calculated by the following equation [18,19].

$$\alpha = \frac{(W_0 - W_t)}{\left(W_0 - W_f\right)}, \tag{1}$$

where W_0, W_t, and W_f are the initial polymer weight, the polymer weight at time t, and the polymer weight at the end of the degradation reaction, respectively. The thermal decomposition rate of the samples at given heating rates were obtained by the equation below [20,21].

$$\frac{d\alpha}{dt} = k(T)f(\alpha),\tag{2}$$

In the equation above, $f(\alpha)$ is the reaction model and $k(T)$ is its rate constant, which is expressed based on the *Arrhenius* equation as [22,23]:

$$k(T) = A exp\left(-\frac{E_a}{RT}\right),\tag{3}$$

where A is the pre-exponential factor, R is the universal gas constant, and E_α is the activation energy of the thermal decomposition reaction. By substituting Equation (3) into Equation (2), we obtained the thermal decomposition rate as [24,25]:

$$\frac{d\alpha}{dt} = A exp\left(-\frac{E_a}{RT}\right)f(\alpha),\tag{4}$$

Application of iso-conversional model-free methods is an easy approach to evaluate the complex decomposition process of polymers across the whole temperature range since they are not dependent on model-fitting to estimate the kinetic parameters such as E_α and frequency factor (A) [26–28]. In these methods, the thermal decomposition rate was monotonically considered to be dependent on the temperature (T) at a given degree of degradation. Rearrangement of Equation (4) gives the approximation-free *Friedman* method, which is a differential iso-conversional technique to calculate the activation energy as a function of decomposition degree at each heating rate from the slope of the set of lines obtained through plotting $ln(d\alpha/dt)$ vs. $1/T$ based on experimental data [29,30].

$$ln\left(\frac{d\alpha}{dt}\right) = ln[Af(\alpha)] - \frac{E_\alpha}{RT},\tag{5}$$

Due to the deviations and inaccuracies normally accompanied by numerical differentiation of TGA data, integral iso-conversional methods were preferred in order to predict the thermal decomposition trend. Flynn-Wall-Ozawa (*FWO*) [31] and Kissinger–Akahira–Sunose (*KAS*) [32] are among the integral methods according to which the activation energy of the reaction can be calculated from the slope of the straight lines obtained by plotting $ln(\beta_i)$ vs. $1/T_\alpha$ (Equation (5)) and $ln(\beta_i/T^2{}_{\alpha,i})$ vs. $1/T_\alpha$ (Equation (6)) where the subscript i represent each heating rate, respectively.

$$ln(\beta_i) = Const - 1.052\left(\frac{E_\alpha}{RT_\alpha}\right),\tag{6}$$

$$ln\left(\frac{\beta_i}{T^2_{\alpha,i}}\right) = Const - \left(\frac{E_\alpha}{RT_\alpha}\right),\tag{7}$$

Moreover, the *m-CR* method is used as the other integral method to estimate the activation energy of the thermal degradation reaction.

$$ln\left[\frac{\beta}{T^2(1 - 2RT/E_\alpha)}\right] = ln\left[\frac{-AR}{E_\alpha ln(1 - \alpha)}\right] - \frac{E_\alpha}{RT},\tag{8}$$

The $E\alpha$ values obtained from other methods mentioned above can be used as the first guess to iteratively solve this equation.

Another essential step in studying the kinetics of a reaction, the decomposition reaction of PU is to correctly determine $f(\alpha)$ and, consequently, the reaction order. For the autocatalytic reactions, which

are more complex [33,34], the *Sestak-Berggren* reaction model can be proposed [35,36], according to which two different reaction orders are considered for simultaneously occurring non-catalytic (*n*) and autocatalytic (*m*) reactions.

$$f(\alpha) = \alpha^m (1-\alpha)^n,$$ (9)

Considering one of these models as the reaction mode, one can determine kinetic parameters such as frequency factor (*A*) and reaction orders based on the activation energy values previously obtained by the iso-conversional methods. A common approach to validate these predications is to plot the decomposition rate as a function of temperature both experimentally and theoretically, and compare the results to determine the one in the most agreement with the experimental values.

3. Results

As a clue to understand the dominant morphology and dispersion state, the SEM image of polyurethane nanocomposites containing different amounts of nanoclay is demonstrated in Figure 1. The bright spots are shown by red circles on the images corresponding to clay aggregates. The nano-clay particles are almost finely dispersed in the material. The large clay aggregates can easily be detected in SEM images. No aggregation can be observed in the PU/Nanoclay-1 system, while small aggregates can be observed at the 3 wt.% nano-clay incorporated PU matrix. On the other hand, 5 wt.% clay incorporated PU shows more aggregates in number. Overall, we can see that SEM cannot detect the finest dispersion because of a difference in scattering density of clay and PU matrix. Therefore, the mechanical and thermal properties can be considered as indirect measures of the microstructure changes [37].
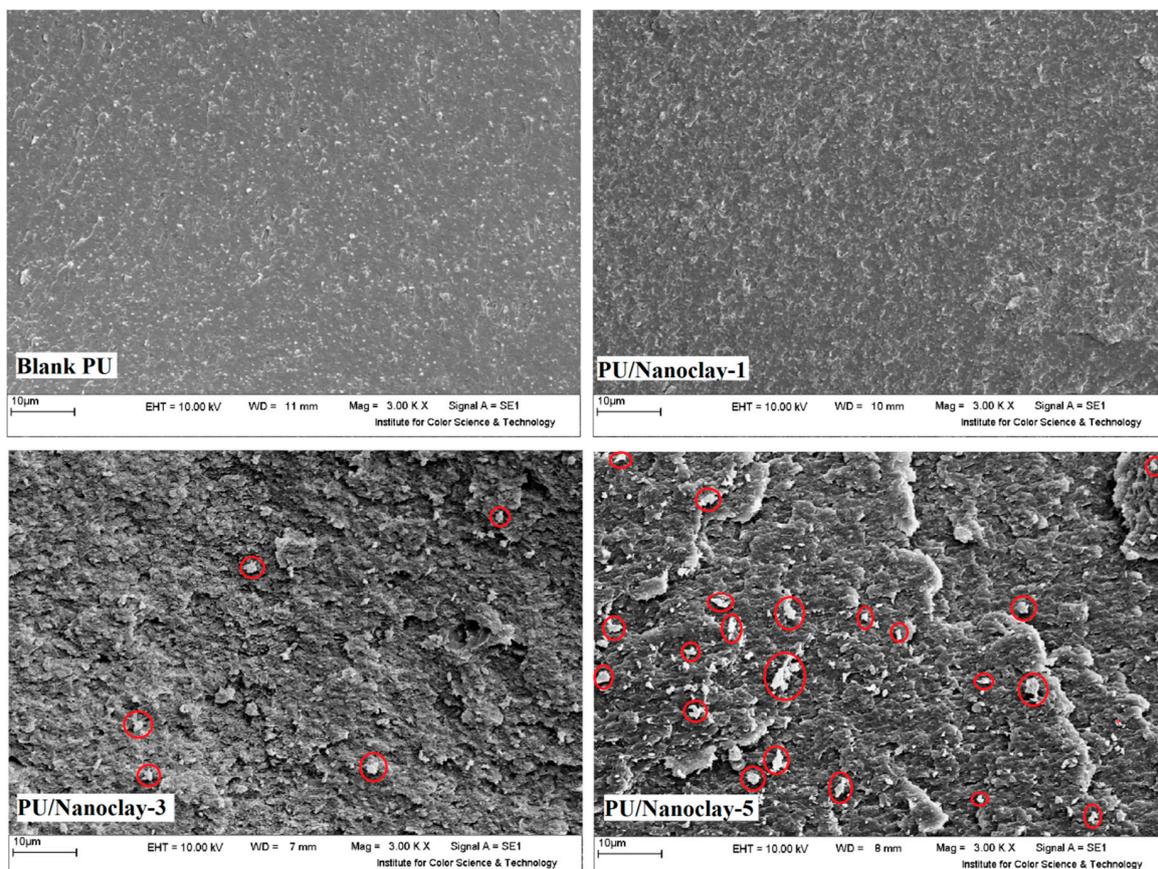
Figure 1. SEM micrographs of blank PU and its nanocomposites containing 1, 3, and 5 wt.% of nano-clay. Red circles show the nano-clay agglomeration.

The SEM micrographs of the blank sample and the sample that contains 1 wt.% nano-clay show smooth surfaces. This is due to the good dispersion and distribution of nano-clay inside the matrix at a low amount of clay. The morphology changes for the samples with higher loadings show large aggregates instead [38,39]. It can be observed that concentrated PU/clay composites have a rougher cross-sectional surface. This observation gives rise to the conclusion that agglomerations exist in the coatings containing 3 wt.% and 5 wt.% nano-clay, as some of them are visible in Figure 1. Nevertheless, more coarseness of the surface in PU/Nanoclay-5 results in a deformed portion due to the high agglomeration of clay particles. Moreover, the higher ability of stress dissipation in nanocomposites at higher loadings can be understood from the increased roughness of the surface, which may be attributed to the weak interactions among the coating matrix and nanoplates aggregations [40].

The thermal behavior of the blank PU and the prepared nanocomposite samples was examined by TGA and DTG (differential thermogravimetric) analysis (Figure 2). At high heating rates, due to the higher kinetic energy per molecules, softening of PU accelerated thermal decomposition. The initial decomposition temperature was shifted to higher values to compensate for shorter time. Thus, the heating rate can affect the thermal degradation behavior [41]. Based on the data provided by the analyses, thermal decomposition characteristics of the system are calculated and reported in Table 1. The degradation temperature at 5% ($T_{5\%}$) and 10% ($T_{10\%}$) weight loss, temperature at maximum weight loss rate (T_P), and char yield or Residue (%) at 600 °C were recorded and interpreted. It is observed that the major decomposition reaction of PU occurs above 300 °C, which is attributed to degradation of soft segments. The minor weight loss in the range of 150 to 250 °C suggests degradation of hard segments and evaporation of volatile compounds [42–45]. Addition of nano-clay stabilized thermal decomposition of the matrix and the TGA curves of nanocomposites were very much similar to the one for pure PU. The decompositions taking place in the region of 150–250 °C for PU nanocomposites is likely due to the evolution of water trapped in between the aluminosilicates' layers (interlayer residing water) [46]. When comparing the results of the nanocomposites to those of the reference sample, one can realize that $T_{5\%}$ and $T_{10\%}$ are significantly increased (more than to 40 °C for $T_{5\%}$ and up to 20 °C for $T_{10\%}$) in all the PU/Clay nanocomposites. This demonstrates the important role of silicate nano-layers to retard the emergence of the decomposition process by impeding the permeability of degradation products [47]. There is evidence that nano-clay prevents quick heat diffusion and limits further degradation [48]. The thermal stability of nano-clay can be explained by a Labyrinth barrier effect, which is generated by the highly anisotropic layered silicate platelets well dispersed in the PU matrix. This can hinder the diffusion of the volatile degradation products including CO_2, CO, and H_2O from the bulk of the PU matrix to the gaseous phase [49].

Table 1. Thermal decomposition characteristics of PU/Clay nanocomposites derived from TGA diagrams at β = 5 °C/min.

Designation	$T_{5\%}$ (°C)	$T_{10\%}$ (°C)	T_P (°C)	Residue (%)
Blank PU	235.3	309.1	372.8	21.8
PU/Nanoclay-1	277.4	328.1	365.2	30.2
PU/Nanoclay-3	269.3	322.3	365.8	28.7
PU/Nanoclay-5	274.3	320.1	362.4	19.8

The maximum values for the initial decomposition temperatures are recorded for the PU/Nanoclay-1 (Figure 1), which shows uniform dispersion of nanoplates in the polymeric matrix, and, accordingly, stronger interaction between them. This observation confirms the significance of good dispersion in nanocomposite systems to achieve superior properties even in low loadings since aggregation of nanomaterials causes void formation in the system, which deteriorates its performance. This point is also reflected in char formation of the nanocomposites at 600 °C and, as it is observed, PU/Nanocaly-5 did not expose any improvement when compared to a pure sample while, for the other

nanocomposite samples, the residual char content increased due to the hindrance effect of nano-clay on the decomposition reaction. The T_P value, being representative of the temperature at which the rate of degradation is a maximum, is considered as the peak value of the DTG thermograms. Introduction of nano-clay to PU slightly shifted T_P to lower temperatures for all the nanocomposites, which means that the nano-clay accelerated the chain scission reactions of polyurethane. However, from similarity of T_P values for PU/Nanoclay-1 and PU/Nanoclay-3, one can infer that higher amounts of nano-clay would provide a good protection barrier against degradation if a good dispersion prerequisite is met [50].
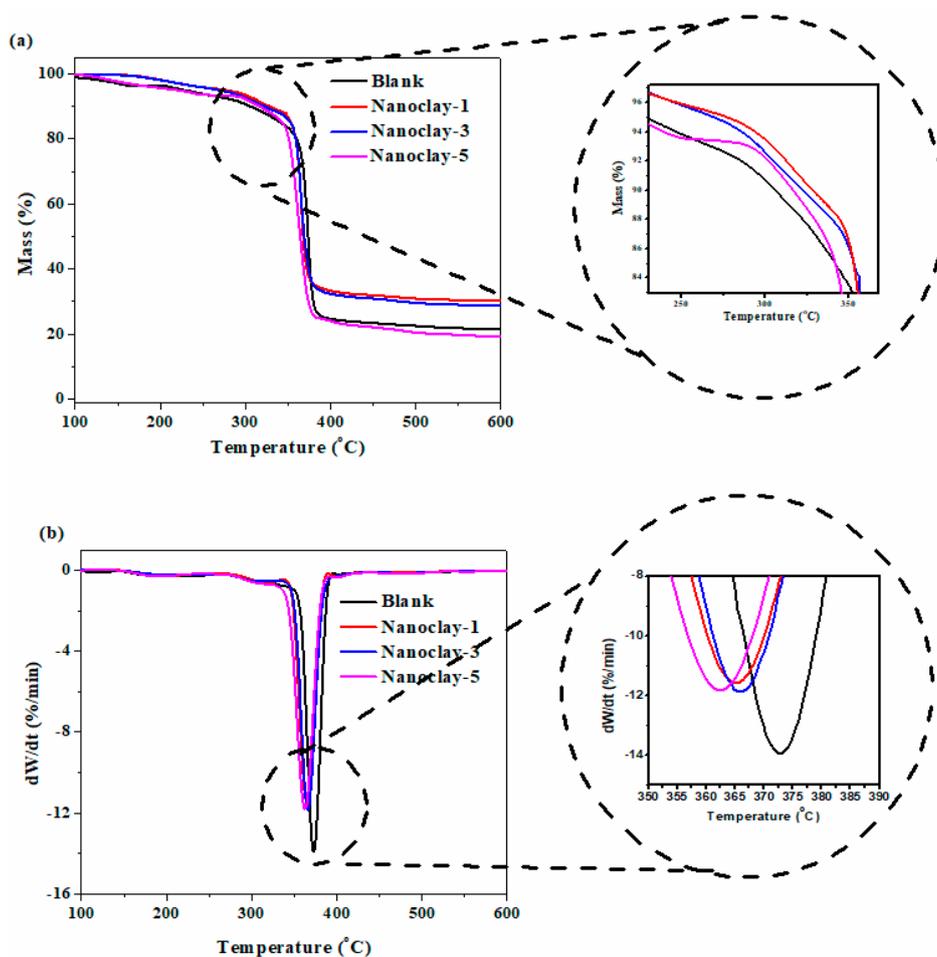

Figure 2. (**a**,**b**) TGA and DTG thermograms of PU/Clay nanocomposites at β = 5 °C/min.

The partial mass loss (α) as a function of temperature is calculated according to Equation (1) and depicted in Figure 3. The general shape of the curves is similar for all the samples at all the heating rates, which shows that the presence of the clay nanoplates in the system do not affect the decomposition mechanism of PU. It is observed that, by increasing the heating rate of the analysis, the curves shift to the higher temperatures regardless of the type of the sample. As a result, it can be concluded that the decomposition reaction depends on the heating rate.

Figure 4 demonstrates the set of straight lines, which are obtained by *Friedman* (Figure 4a), *KAS* (Figure 4b), *FWO* (Figure 4c), and *m-CR* (Figure 4d) methods in order to calculate activation energy. Figure 4a confirms the claim that applying a differential *Friedman* method on integral TGA data leads to erroneous results, which cannot model the PU decomposition behavior precisely. The other integral methods follow a similar trend and result in comparable values for E_α. The calculated activation energy by each method is plotted against partial mass loss (Figure 5) to facilitate its interpretation throughout the reaction.
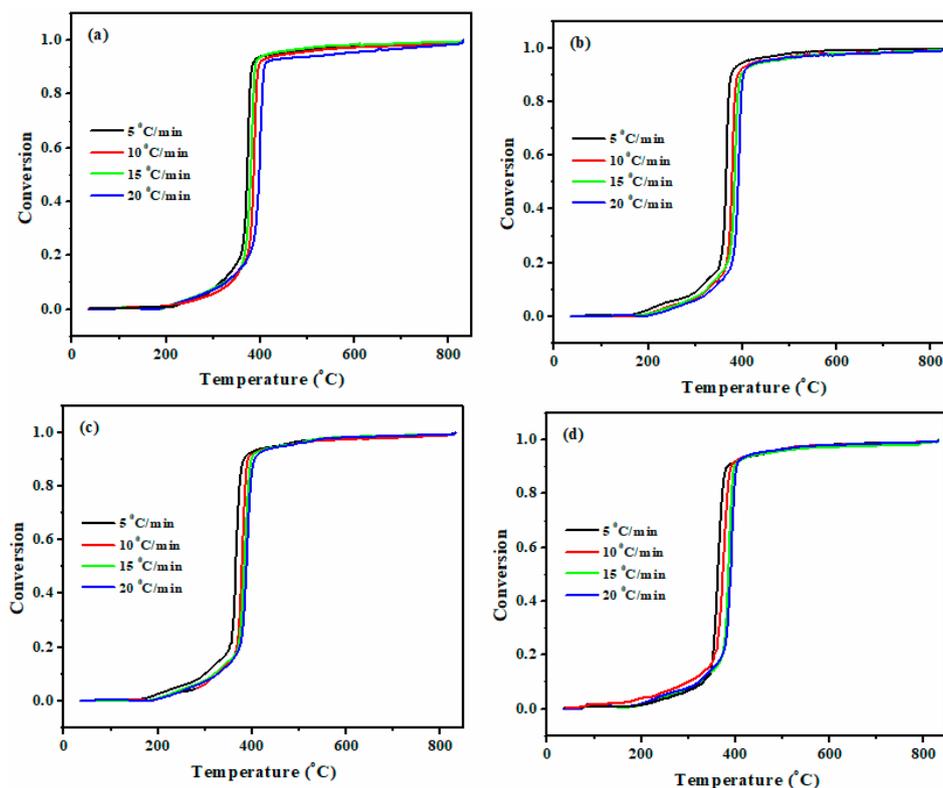
Figure 3. Degradation conversion profiles of nanocomposites at various heating rates for (**a**) blank PU, (**b**) PU/Nanoclay-1, (**c**) PU/Nanoclay-3, and (**d**) PU/Nanoclay-5.
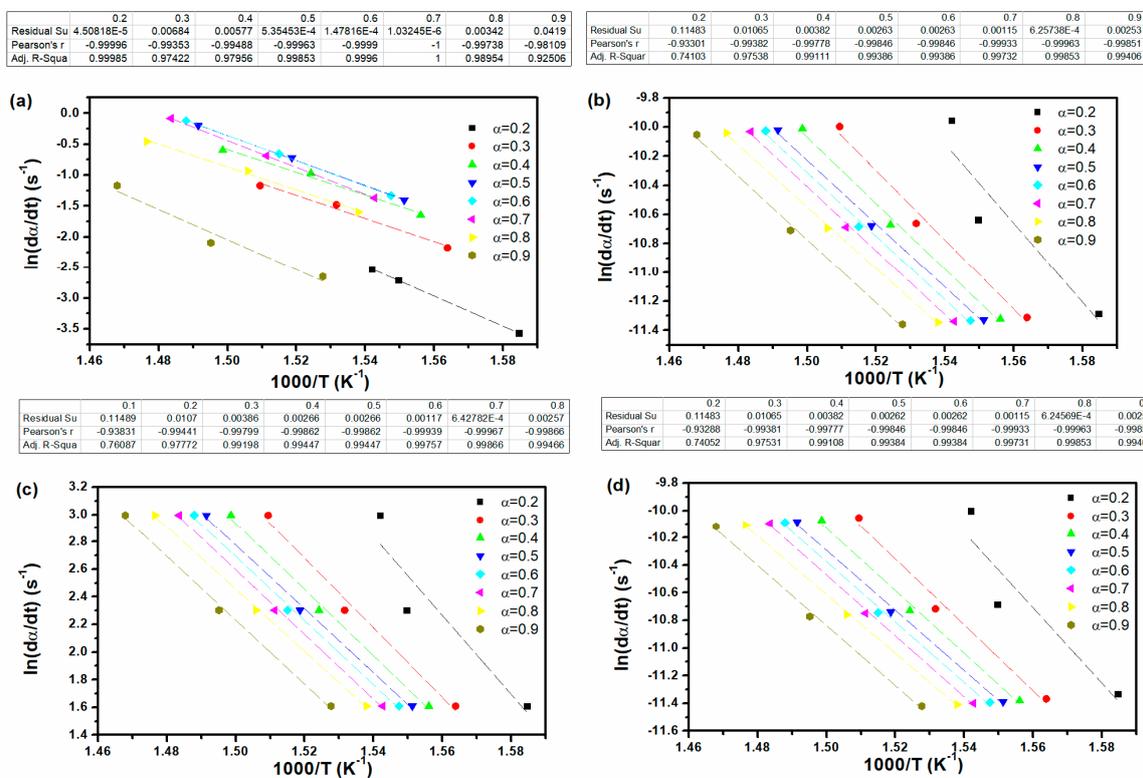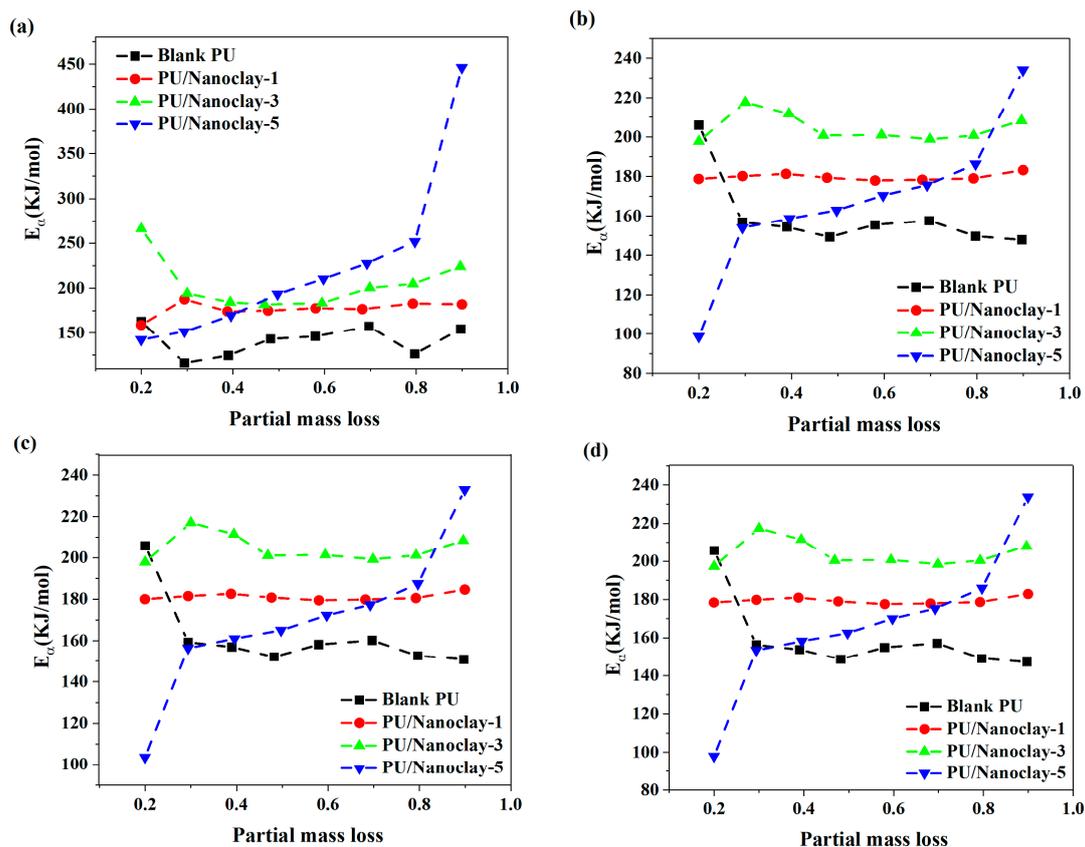

Figure 4. Typical iso-conversional plots for PU/Clay nanocomposites (**a**) *Friedman*, (**b**) *KAS*, (**c**) *FWO*, and (**d**) *m-CR* methods.

Figure 5. Activation energy of blank PU and its nanocomposites containing 1, 3, and 5 wt.% of nano-clay in terms of partial mass loss obtained using (**a**) *Friedman* (**b**) *KAS*, (**c**) *FWO*, and (**d**) *m-CR* methods.

Putting Figure 5 under scrutiny, one can realize that, in the α range of more than 0.2, the activation energy of the PU/Clay nanocomposites' degradation reaction is increased irrespective of nanoplates concentration in the matrix and the applied iso-conversional method. Thus, the presence of nano-clay has an inhibitory role on the decomposition reaction of PU and it becomes more significant when its amount is increased in the system. This behavior can be attributed to restricted mobility of PU chains in the interaction with nano-clay and barrier effect of nanoplates on the degradation of intercalated polymers trapped between interlayers of clay. A noteworthy observation is that, for all the samples except from PU/Nanoclay-5, the value of E_α is almost constant in the course of reaction while, for the highest loading of nano-clay, an ascending behavior is noticeable for E_α. However, its value is lower than that of other samples with lower loading, which is indicative of lower effectiveness of nanoplates on retarding the decomposition process. This observation confirms the negative effect of inconsistent dispersion on performance of the nanocomposites.

The reaction model $f(\alpha)$ was determined by Criados master plots [51], expression:

$$\frac{Z(\alpha)}{Z(0.5)} = \frac{f(\alpha)g(\alpha)}{f(0.5)g(0.5)} = \left(\frac{T_\alpha}{T_{0.5}}\right)^2 \frac{(d\alpha/dt)_\alpha}{(d\alpha/dt)_{0.5}} \tag{10}$$

By the Criado method, experimental TGA results can be compared with the reaction models, $f(\alpha)$ and $g(\alpha)$, as shown in Table 2. In Equation (10), $T_{0.5}$ and $(d\alpha/dt)_{0.5}$ indicate the temperature and degradation rate at $\alpha = 0.5$. The right-hand side of Equation (10) can be calculated from the experimental data. The left-hand side of Equation (10) means $[(f(\alpha)g(\alpha))/f(0.5)g(0.5)]$ represents the theoretical master plots obtained from reaction models in Table 2.

Table 2. Reaction models of the most common reaction mechanism [52,53].

Reaction Model	$f(\alpha)$	$g(\alpha)$	Model Code
Power law	$2\alpha^{1/2}$	$\alpha^{1/2}$	P2
Power law	$3\alpha^{2/4}$	$\alpha^{1/3}$	P3
Power law	$4\alpha^{3/4}$	$\alpha^{1/4}$	P4
Avrami-Erofeev: Two-dimensional nucleation	$2(1-\alpha)[-\ln(1-\alpha)]^{1/2}$	$[-\ln(1-\alpha)]^{1/2}$	A2
Avrami-Erofeev: Three-dimensional nucleation	$3(1-\alpha)[-\ln(1-\alpha)]^{2/4}$	$[-\ln(1-\alpha)]^{1/3}$	A3
Avrami-Erofeev: Four-dimensional nucleation	$4(1-\alpha)[-\ln(1-\alpha)]^{3/4}$	$[-\ln(1-\alpha)]^{1/4}$	A4
Contracting cylinder: Two-dimensional phase boundary reaction	$2(1-\alpha)^{1/2}$	$1-(1-\alpha)^{1/2}$	R2
Contracting sphere: Three-dimensional phase boundary reaction	$3(1-\alpha)^{2/3}$	$1-(1-\alpha)^{1/3}$	R3
Two-dimensional diffusion	$[-\ln(1-\alpha)]^{-1}$	$(1-\alpha)\ln(1-\alpha)+\alpha$	D2
Three-dimensional diffusion	$3/2(1-\alpha)^{2/3}[1-(1-\alpha)^{1/3}]^{-1}$	$[1-(1-\alpha)^{1/3}]^2$	D3
Mampel (first order)	$1-\alpha$	$-\ln(1-\alpha)$	F1
One-dimensional diffusion	$1/2\alpha^{-1}$	α^2	D1
Ginstling-Brounshtein	$3/2((1-\alpha)^{-1/3}-1)$	$1-(2\alpha/3)-(1-\alpha)^{2/3}$	D4
Second order	$(1-\alpha)^2$	$(1-\alpha)^{-1}-1$	F2
Third order	$(1-\alpha)^3$	$[(1-\alpha)^{-1}-1]/2$	F3

By comparing theoretical and experimental plots, the most appropriate reaction model can be obtained. The theoretical master plots of $z(\alpha)/z(0.5)$ as a function of α for different mechanisms (Table 2) along with experimental reduced plots for blank PU and its nanocomposites are illustrated in Figure 6 at a heating rate of 5 °C/min. The reaction model for a system of multiple complex reactions has little meaning. Yet, the reaction model was predicted to comprehend the apparent reaction model. As can be seen from Figure 6, the degradation kinetic models for blank PU, PU/nanoclay-1, PU/nanoclay-3, and PU/nanoclay-5 were found to be D4 for the conversion values from 0.1 to 0.5. The data was fitting with the R2 model for blank PU, PU/nanoclay-1, and PU/nanoclay-5 and F2 for PU/nanoclay-3 in the conversion range of 0.5–0.8.
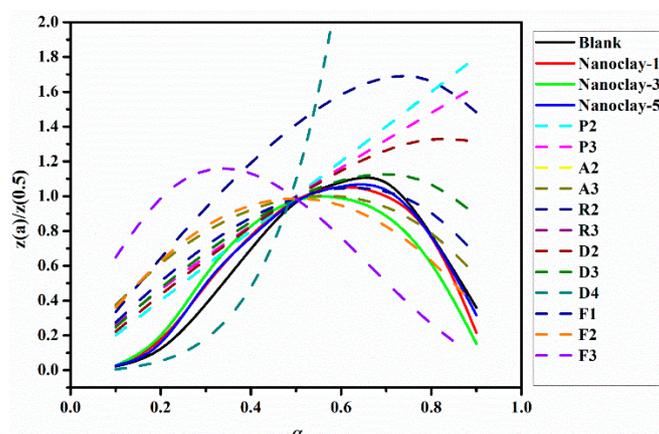
Figure 6. Theoretical master plots of different reaction models and experimental reduced rate plot at 5 °C/min for blank PU and its prepared nanocomposites.

According to Equation (8), kinetic parameters of *A* and reaction orders are calculated based on the *Sestak-Berggren* model using *Friedman*, *KAS*, *FWO*, and *m-CR* iso-conversional methods, which are presented in Table 3. Since the frequency factor is directly dependent on E_α [54], it shows the same variations and expresses that the rate of component vibration in the system is increased by rising in E_α. It is clear that, in the presence of nano-clay, the energy dissipation of PU chains enhances and the system develops stability against a temperature rise. The energy dissipation is boosted by growth in the nanoplates amount, but a lack of proper dispersion in the PU/Nanoclay-5 sample prevents it from following the pattern. The values obtained by all the integral methods are equal in both reaction models with a good approximation. An increase in *n* value due to the introduction of nano-clay to PU matrix indicates that the reaction is accelerated. Considering the *Sestak-Berggren* reaction model, one can realize that the same behavior can be assigned to *m* as a catalytic reaction order with regard to concentration variations. Again, the sample containing the highest content of nano-clay is accepted because of its dispersion state.

Table 3. Decomposition parameters based on the *Sestak-Berggren* decomposition reaction of PU nanocomposites calculated using different iso-conversional kinetic models.

Designation		Blank PU	PU/Nanoclay-1	PU/Nanoclay-3	PU/Nanoclay-5
Friedman	$E\alpha$ (kJ/mol.)	173.37	180.16	203.44	219.19
	$Ln\ A$ (min^{-1})	36.05	38.23	43.83	44.89
	n	3.59	3.77	4.56	2.86
	m	3.68	4.19	5.42	4.50
KAS	$E\alpha$ (kJ/mol.)	189.91	175.84	202.77	173.39
	$Ln\ A$ (min^{-1})	39.08	37.43	43.70	36.11
	n	3.53	3.78	4.56	2.87
	m	3.68	4.19	5.42	4.31
FWO	$E\alpha$ (kJ/mol.)	190.90	177.43	203.03	175.09
	$Ln\ A$ (min^{-1})	39.27	37.72	43.75	36.43
	n	3.53	3.77	4.56	2.87
	m	3.67	4.19	5.42	4.31
m-CR	$E\alpha$ (kJ/mol.)	189.57	175.49	202.47	173.02
	$Ln\ A$ (min^{-1})	39.02	37.36	43.65	36.03
	n	3.53	3.77	4.56	2.87
	m	3.68	4.19	5.42	4.31

For validation of obtained theoretical models, the rate of decomposition reaction is plotted against temperature in order to find the best-fitted model to the experimental data, which are demonstrated in Figure 7 for the *Sestak-Berggren* model. The two kinetic exponents of the *Sestak-Berggren* model provide a closer estimation pattern to the actual case, especially in the early stage of the temperature window.
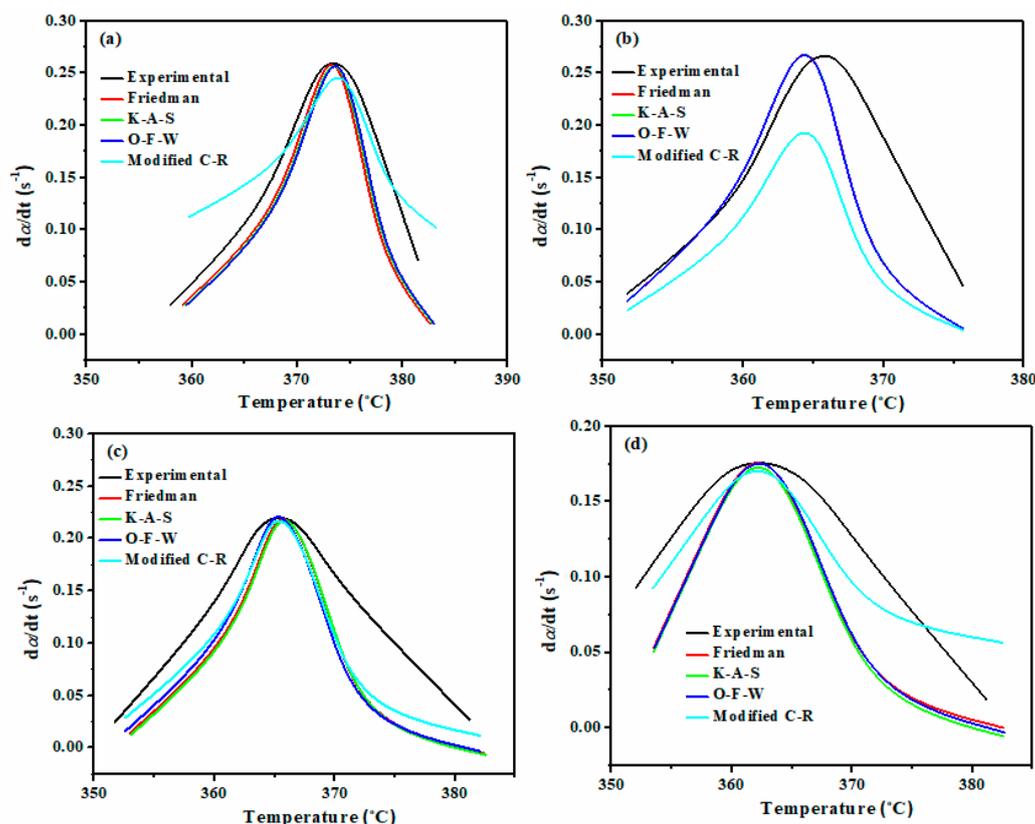
Figure 7. Predicted kinetics plots based on the *Sestak Berggren* decomposition reaction model for blank PU and its nanocomposites containing various nano-clay loadings at the heating rate of 5 °C/min, (**a**) blank PU, (**b**) PU/Nanoclay-1, (**c**) PU/Nanoclay-3, and (**d**) PU/Nanoclay-5.

4. Conclusions

This work aimed to provide a kinetic study on the decomposition reaction of the PU polymer containing different amounts of nano-clay by taking advantage of TGA analysis. It was revealed that:

- The presence of nano-clay in the system enhanced the PU thermal stability;
- The performance of the nanocomposite is extremely dependent on the dispersion state of the nano-clay in the PU matrix;
- The SEM images demonstrated that some aggregations exist in the nanocomposite with the highest loading while the morphologies of nanocomposites containing 1% and 3% nano-clay were uniform;
- The thermal stability of the nanocomposites had an ascending behavior by increasing nano-clay content from 1 to 3 wt.%. However, it descended when the concentration of the nano-clay reached to 5 wt.% due to aggregation of nanoplates in this content;
- The initial decomposition temperature of the systems considerably increased (more than 40 °C for $T_{5\%}$) due to the barrier effect of the nano-clay;
- The char content of the samples containing uniformly dispersed nanoplates was enhanced up to 10% at 600 °C;
- The value of E_α, which was calculated based on the TGA data and model-free iso-conversional methods including *Friedman*, *FWO*, *KAS*, and *m-CR* increased for all the nanocomposite sample in comparison to the pure one, which confirmed greater thermal resistance of the system against elevated temperatures;
- The *Sestak-Berggren* model well-fitted the experimental curve of the reaction rate, specifically in lower temperatures.

It can be concluded that the introduction of nano-clay to PU polymer improves its thermal properties and the best dispersion method should be taken into consideration to achieve desirable results. The polyurethane decomposition process is an auto-catalytic reaction, which should be regarded when studying its kinetic behavior.

Conflicts of Interest: The authors declare no conflict of interest. The funders had no role in the design of the study, in the collection, analyses, or interpretation of data, in the writing of the manuscript, or in the decision to publish the results.

References

1. Celina, M.C. Review of polymer oxidation and its relationship with materials performance and lifetime prediction. *Polym. Degrad. Stab.* **2013**, *98*, 2419–2429. [CrossRef]
2. Jiao, L.; Xiao, H.; Wang, Q.; Sun, J. Thermal degradation characteristics of rigid polyurethane foam and the volatile products analysis with TG-FTIR-MS. *Polym. Degrad. Stab.* **2013**, *98*, 2687–2696. [CrossRef]
3. Krongauz, V.V. Crosslink density dependence of polymer degradation kinetics: Photocrosslinked acrylates. *Thermochim. Acta* **2010**, *503–504*, 70–84. [CrossRef]
4. Igor, V.K.; David, R.Z.; Nicholas, J.T. Polyurethane nanocomposites. *Des. Monomers Polym.* **2009**, *12*, 279–290. [CrossRef]
5. Khobragade, P.S.; Hansora, D.P.; Naik, J.B.; Chatterjee, A. Flame retarding performance of elastomeric nanocomposites: A review. *Polym. Degrad. Stab.* **2016**, *130*, 194–244. [CrossRef]
6. Karami, Z.; Jouyandeh, M.; Ali, J.A.; Ganjali, M.R.; Aghazadeh, M.; Maadani, M.; Rallini, M.; Luzi, F.; Torre, L.; Puglia, D.; et al. Cure Index for labeling curing potential of epoxy/LDH nanocomposites: A case study on nitrate anion intercalated Ni-Al-LDH. *Prog. Org. Coat.* **2019**, *136*, 105228. [CrossRef]
7. Vaithylingam, R.; Ansari, M.N.M.; Shanks, R.A. Recent Advances in Polyurethane Based Nanocomposites: A Review. *Polym. Plast. Technol. Eng.* **2017**, *56*, 1528–1541. [CrossRef]
8. Haghayegh, M.; Mir Mohamad Sadeghi, G. Synthesis of shape memory polyurethane/clay nanocomposites and analysis of shape memory, thermal, and mechanical properties. *Polym. Compos.* **2012**, *33*, 843–849. [CrossRef]
9. Peng, S.; Iroh, J.O. Synthesis and characterization of crosslinked polyurethane/clay nanocomposites. *J. Appl. Polym. Sci.* **2016**, *133*. [CrossRef]
10. Rehab, A.; Salahuddin, N. Nanocomposite materials based on polyurethane intercalated into montmorillonite clay. *Mater. Sci. Eng. A* **2005**, *399*, 368–376. [CrossRef]
11. Chen-Yang, Y.W.; Yang, H.C.; Li, G.J.; Li, Y.K. Thermal and anticorrosive properties of polyurethane/clay nanocomposites. *J. Polym. Res.* **2004**, *11*, 275–283. [CrossRef]
12. Wang, X.-C.; Geng, T.; Han, J.; Liu, C.-T.; Shen, C.-Y.; Turng, L.-S.; Yang, H.E. Effects of nanoclays on the thermal stability and flame retardancy of microcellular thermoplastic polyurethane nanocomposites. *Polym. Compos.* **2018**, *39*, E1429–E1440. [CrossRef]
13. Maciejewski, M. Computational aspects of kinetic analysis.: Part B: The ICTAC Kinetics Project—The decomposition kinetics of calcium carbonate revisited, or some tips on survival in the kinetic minefield. *Thermochim. Acta* **2000**, *355*, 145–154. [CrossRef]
14. Jomaa, G.; Goblet, P.; Coquelet, C.; Morlot, V. Kinetic modeling of polyurethane pyrolysis using non-isothermal thermogravimetric analysis. *Thermochim. Acta* **2015**, *612*, 10–18. [CrossRef]
15. Pashaei, S.; Siddaramaiah; Syed, A.A. Thermal degradation kinetics of polyurethane/organically modified montmorillonite clay nanocomposites by TGA. *J. Macromol. Sci. Part A* **2010**, *47*, 777–783. [CrossRef]
16. Zhao, Y.; Mo, H.; Jiang, X.; Han, B.; Feng, F.; Wang, D.; Fu, L.; He, L.; Zhang, J.; Shen, J. Thermal stability and thermal oxidation kinetics of PU/CA-MMT composites. *J. Appl. Polym. Sci.* **2019**, *136*, 47002. [CrossRef]
17. Pau, D.S.W.; Fleischmann, C.M.; Spearpoint, M.J.; Li, K.Y. Determination of kinetic properties of polyurethane foam decomposition for pyrolysis modelling. *J. Fire Sci.* **2013**, *31*, 356–384. [CrossRef]

18. Bockhorn, H.; Hornung, A.; Hornung, U. Mechanisms and kinetics of thermal decomposition of plastics from isothermal and dynamic measurements. *J. Anal. Appl. Pyrolysis* **1999**, *50*, 77–101. [CrossRef]

19. Paran, S.M.R.; Vahabi, H.; Jouyandeh, M.; Ducos, F.; Formela, K.; Saeb, M.R. Thermal decomposition kinetics of dynamically vulcanized polyamide 6–acrylonitrile butadiene rubber–halloysite nanotube nanocomposites. *J. Appl. Polym. Sci.* **2019**, *136*, 47483. [CrossRef]

20. Yao, F.; Wu, Q.; Lei, Y.; Guo, W.; Xu, Y. Thermal decomposition kinetics of natural fibers: Activation energy with dynamic thermogravimetric analysis. *Polym. Degrad. Stab.* **2008**, *93*, 90–98. [CrossRef]

21. Jouyandeh, M.; Ganjali, M.R.; Ali, J.A.; Aghazadeh, M.; Paran, S.M.R.; Naderi, G.; Saeb, M.R.; Thomas, S. Curing epoxy with polyvinylpyrrolidone (PVP) surface-functionalized $Zn_xFe_{3-x}O_4$ magnetic nanoparticles. *Prog. Org. Coat.* **2019**, *136*, 105227. [CrossRef]

22. Tikhani, F.; Moghari, S.; Jouyandeh, M.; Laoutid, F.; Vahabi, H.; Saeb, M.R.; Dubois, P. Curing kinetics and thermal stability of epoxy composites containing newly obtained nano-scale aluminum hypophosphite $(AlPO_2)$. *Polymers* **2020**, *12*, 644. [CrossRef] [PubMed]

23. Jouyandeh, M.; Zarrintaj, P.; Ganjali, M.R.; Ali, J.A.; Karimzadeh, I.; Aghazadeh, M.; Ghaffari, M.; Saeb, M.R. Curing epoxy with electrochemically synthesized $Gd_xFe_{3-x}O_4$ magnetic nanoparticles. *Prog. Org. Coat.* **2019**, *136*, 105245. [CrossRef]

24. Jouyandeh, M.; Ganjali, M.R.; Seidi, F.; Xiao, H.; Saeb, M.R. Nonisothermal cure kinetics of epoxy/ polyvinylpyrrolidone functionalized superparamagnetic nano-Fe_3O_4 composites: Effect of Zn and Mn doping. *J. Compos. Sci.* **2020**, *4*, 55. [CrossRef]

25. Jouyandeh, M.; Paran, S.M.R.; Khadem, S.S.M.; Ganjali, M.R.; Akbari, V.; Vahabi, H.; Saeb, M.R. Nonisothermal cure kinetics of epoxy/$Mn_xFe_{3-x}O_4$ nanocomposites. *Prog. Org. Coat.* **2020**, *140*, 105505. [CrossRef]

26. Rastin, H.; Saeb, M.R.; Nonahal, M.; Shabanian, M.; Vahabi, H.; Formela, K.; Gabrion, X.; Seidi, F.; Zarrintaj, P.; Sari, M.G.; et al. Transparent nanocomposite coatings based on epoxy and layered double hydroxide: Nonisothermal cure kinetics and viscoelastic behavior assessments. *Prog. Org. Coat.* **2017**, *113*, 126–135. [CrossRef]

27. Nonahal, M.; Rastin, H.; Saeb, M.R.; Sari, M.G.; Moghadam, M.H.; Zarrintaj, P.; Ramezanzadeh, B. Epoxy/PAMAM dendrimer-modified graphene oxide nanocomposite coatings: Nonisothermal cure kinetics study. *Prog. Org. Coat.* **2018**, *114*, 233–243. [CrossRef]

28. Seidi, F.; Jouyandeh, M.; Akbari, V.; Paran, S.M.R.; Livi, S.; Ducos, F.; Vahabi, H.; Ganjali, M.R.; Saeb, M.R. Super-crosslinked ionic liquid-intercalated montmorillonite/epoxy nanocomposites: Cure kinetics, viscoelastic behavior and thermal degradation mechanism. *Polym. Eng. Sci.* **2020**, *60*, 1940–1957. [CrossRef]

29. Friedman, H.L. Kinetics of thermal degradation of char-forming plastics from thermogravimetry. Application to a phenolic plastic. *J. Polym. Sci. Part C Polym. Symp.* **1964**, *6*, 183–195. [CrossRef]

30. Jouyandeh, M.; Ganjali, M.R.; Ali, J.A.; Aghazadeh, M.; Stadler, F.J.; Saeb, M.R. Curing epoxy with electrochemically synthesized $Ni_xFe_{3-x}O_4$ magnetic nanoparticles. *Prog. Org. Coat.* **2019**, *136*, 105198. [CrossRef]

31. Venkatesh, M.; Ravi, P.; Tewari, S.P. Isoconversional kinetic analysis of decomposition of nitroimidazoles: Friedman method vs Flynn-Wall-Ozawa method. *J. Phys. Chem. A* **2013**, *117*, 10162–10169. [CrossRef] [PubMed]

32. Kissinger, H.E. Reaction kinetics in differential thermal analysis. *Anal. Chem.* **1957**, *29*, 1702–1706. [CrossRef]

33. Jouyandeh, M.; Karami, Z.; Ali, J.A.; Karimzadeh, I.; Aghazadeh, M.; Laoutid, F.; Vahabi, H.; Saeb, M.R.; Ganjali, M.R.; Dubois, P. Curing epoxy with polyethylene glycol (PEG) surface-functionalized $Ni_xFe_{3-x}O_4$ magnetic nanoparticles. *Prog. Org. Coat.* **2019**, *136*, 105250. [CrossRef]

34. Jouyandeh, M.; Karami, Z.; Hamad, S.M.; Ganjali, M.R.; Akbari, V.; Vahabi, H.; Kim, S.-J.; Zarrintaj, P.; Saeb, M.R. Nonisothermal cure kinetics of epoxy/$Zn_xFe_{3-x}O_4$ nanocomposites. *Prog. Org. Coat.* **2019**, *136*, 105290. [CrossRef]

35. Akbari, V.; Jouyandeh, M.; Paran, S.M.R.; Ganjali, M.R.; Abdollahi, H.; Vahabi, H.; Ahmadi, Z.; Formela, K.; Esmaeili, A.; Mohaddespour, A. Effect of surface treatment of halloysite nanotubes (HNTs) on the kinetics of epoxy resin cure with amines. *Polymers* **2020**, *12*, 930. [CrossRef] [PubMed]

36. Jouyandeh, M.; Yarahmadi, E.; Didehban, K.; Ghiyasi, S.; Paran, S.M.R.; Puglia, D.; Ali, J.A.; Jannesari, A.; Saeb, M.R.; Ranjbar, Z. Cure kinetics of epoxy/graphene oxide (GO) nanocomposites: Effect of starch functionalization of GO nanosheets. *Prog. Org. Coat.* **2019**, *136*, 105217. [CrossRef]

37. Kornmann, X.; Lindberg, H.; Berglund, L.A. Synthesis of epoxy–clay nanocomposites: Influence of the nature of the clay on structure. *Polymer* **2001**, *42*, 1303–1310. [CrossRef]

38. Jouyandeh, M.; Tikhani, F.; Shabanian, M.; Movahedi, F.; Moghari, S.; Akbari, V.; Gabrion, X.; Laheurte, P.; Vahabi, H.; Saeb, M.R. Synthesis, characterization, and high potential of 3D metal–organic framework (MOF) nanoparticles for curing with epoxy. *J. Alloys Compd.* **2020**, 15454. [CrossRef]

39. Seidi, F.; Jouyandeh, M.; Taghizadeh, M.; Taghizadeh, A.; Vahabi, H.; Habibzadeh, S.; Formela, K.; Saeb, M.R. Metal-organic framework (MOF)/epoxy coatings: A review. *Materials* **2020**, *13*, 2881. [CrossRef]

40. Jouyandeh, M.; Tikhani, F.; Hampp, N.; Yazdi, D.A.; Zarrintaj, P.; Ganjali, M.R.; Saeb, M.R. Highly curable self-healing vitrimer-like cellulose-modified halloysite nanotube/epoxy nanocomposite coatings. *Chem. Eng. J.* **2020**, *396*, 125196. [CrossRef]

41. Álvarez-Alcón, M.; López de Lacalle, L.N.; Fernández-Zacarías, F. Multiple sensor monitoring of CFRP drilling to define cutting parameters sensitivity on surface roughness, cylindricity and diameter. *Materials* **2020**, *13*, 2796. [CrossRef] [PubMed]

42. Jouyandeh, M.; Ganjali, M.R.; Aghazadeh, M.; Habibzadeh, S.; Formela, K.; Saeb, M.R. Bulk-Surface Modification of Nanoparticles for Developing Highly-Crosslinked Polymer Nanocomposites. *Polymers* **2020**, *12*, 1820. [CrossRef] [PubMed]

43. Hadavand, B.S.; Jouyandeh, M.; Paran, S.M.R.; Khalili, R.; Vahabi, H.; Bafghi, H.F.; Laoutid, F.; Vijayan, P.P.; Saeb, M.R. Silane-functionalized Al$_2$O$_3$-modified polyurethane powder coatings: Nonisothermal degradation kinetics and mechanistic insights. *J. Appl. Polym. Sci.* **2020**, 49412. [CrossRef]

44. Tikhani, F.; Shirkavand Hadavand, B.; Fakharizadeh Bafghi, H.; Jouyandeh, M.; Vahabi, H.; Formela, K.; Hosseini, H.; Paran, S.M.R.; Esmaeili, A.; Mohaddespour, A. Polyurethane/silane-functionalized ZrO$_2$ nanocomposite powder coatings: Thermal degradation kinetics. *Coatings* **2020**, *10*, 413. [CrossRef]

45. Barick, A.; Tripathy, D. Preparation and characterization of thermoplastic polyurethane/organoclay nanocomposites by melt intercalation technique: Effect of nanoclay on morphology, mechanical, thermal, and rheological properties. *J. Appl. Polym. Sci.* **2010**, *117*, 639–654. [CrossRef]

46. Thirumal, M.; Khastgir, D.; Singha, N.K.; Manjunath, B.; Naik, Y. Effect of a nanoclay on the mechanical, thermal and flame retardant properties of rigid polyurethane foam. *J. Macromol. Sci. Part A Pure Appl. Chem.* **2009**, *46*, 704–712. [CrossRef]

47. Cervantes-Uc, J.M.; Moo Espinosa, J.I.; Cauich-Rodríguez, J.V.; Ávila-Ortega, A.; Vázquez-Torres, H.; Marcos-Fernández, A.; San Roman, J. TGA/FTIR studies of segmented aliphatic polyurethanes and their nanocomposites prepared with commercial montmorillonites. *Polym. Degrad. Stab.* **2009**, *94*, 1666–1677. [CrossRef]

48. Xiong, J.; Liu, Y.; Yang, X.; Wang, X. Thermal and mechanical properties of polyurethane/montmorillonite nanocomposites based on a novel reactive modifier. *Polym. Degrad. Stab.* **2004**, *86*, 549–555. [CrossRef]

49. Cheng, A.; Wu, S.; Jiang, D.; Wu, F.; Shen, J. Study of elastomeric polyurethane nanocomposites prepared from grafted organic–montmorillonite. *Colloid Polym. Sci.* **2006**, *284*, 1057–1061. [CrossRef]

50. Ramesh, S.; Punithamurthy, K. The effect of organoclay on thermal and mechanical behvaiours of thermoplastic polyurethane nanocomposites. *Dig. J. Nanomater. Biostruct.* **2017**, *12*, 331–338.

51. Criado, J.M. Kinetic analysis of DTG data from master curves. *Thermochim. Acta* **1978**, *24*, 186–189. [CrossRef]

52. Das, P.; Tiwari, P. Thermal degradation kinetics of plastics and model selection. *Thermochim. Acta* **2017**, *654*, 191–202. [CrossRef]

53. Vyazovkin, S.; Burnham, A.K.; Criado, J.M.; Pérez-Maqueda, L.A.; Popescu, C.; Sbirrazzuoli, N. ICTAC Kinetics Committee recommendations for performing kinetic computations on thermal analysis data. *Thermochim. Acta* **2011**, *520*, 1–19. [CrossRef]

54. Vimalathithan, P.K.; Barile, C.; Casavola, C.; Arunachalam, S.; Battisti, M.G.; Friesenbichler, W.; Vijayakumar, C.T. Thermal degradation kinetics of polypropylene/clay nanocomposites prepared by injection molding compounder. *Polym. Compos.* **2019**, *40*, 3634–3643. [CrossRef]